STATISTICS, OPTIMIZATION AND INFORMATION COMPUTING
Stat., Optim. Inf. Comput., Vol. **x**, Month 202x, pp 0–14.
Published online in International Academic Press (www.IAPress.org)

Implementation of DRBEM with predictor-corrector for infiltration in four layered heterogeneous soil under impermeable and non-impermeable conditions

Millatuz Zahroh*, Deviatul Indah Pramadhani, Moh. Hasan

Department of Mathematics, Universitas Jember, Indonesia

Abstract This research focuses on the steady infiltration problem in a furrow irrigation channel consisting of four heterogeneous soil layers (horizon O, A, B, and C), incorporating the root water uptake process. The rectangular irrigation channel is analyzed under both impermeable and permeable conditions. The problem is formulated as a mathematical model using a non-linear partial differential equation (PDE). After being transformed into a linear PDE, the equation is determined using the Dual Reciprocity Boundary Element Method (DRBEM) combined with a predictor-corrector scheme. The implementation of DRBEM to solve the model is carried out in two stages. In the first stage, the model is solved without considering root water uptake, and the resulting solution is used to estimate the water pressure response function using the predictor-corrector scheme. In the second stage, DRBEM is applied again with the root water uptake process. The numerical solution obtained represents the suction potential value. The study examines the characteristics of water infiltration in the four heterogeneous soil layers influenced by the uptake of root water. The results reveal distinct water movement patterns, with the uppermost layer showing divergent behavior and the lowest layer showing convergent behavior. In addition, infiltration in impermeable and permeable channels shows that the permeable condition results in greater water infiltration. These suggest higher water absorption, leading to an increased soil water content.

Keywords Infiltration, Root Water-Uptake, DRBEM, Predictor-Corrector Scheme, Suction Potential.

DOI: 10.19139/soic-2310-5070-2376

1. Introduction

Indonesia, as an archipelagic country with diverse topography, is vulnerable to natural phenomena and climate change, such as El Nino and the Indian Ocean Dipole (IOD). El Nino is an anomaly in the temperature of the sea surface that leads to a decrease in rainfall levels [1]. Meanwhile, IOD is a large-scale physical phenomenon in the eastern and western Indian Ocean that affects changes in rainfall patterns [3]. Both phenomena can occur simultaneously, increasing the risk of severe drought. Effective water management is required to address and mitigate the impact of droughts. In Indonesia, water is used in various sectors, one of which is agriculture. In agriculture, water is typically utilized in irrigation systems. Infiltration in irrigation systems is a crucial stage, as it manages the water resources needed by crops[4].

Infiltration of water into the soil can be expressed by Darcy's law as

$$q = -K\nabla H \tag{1}$$

where q = water flux, K = unsaturated soil conductivity, and ∇H= hydraulic head gradient [6].

*Correspondence to: Millatuz Zahroh (Email: millatuz@unej.ac.id). Department of Mathematics, University of Jember. Kalimatan Street 37, Jember, East Java, Indonesia (68121).

ISSN 2310-5070 (online) ISSN 2311-004X (print)

Equation (1) can be developed as Richard's Equation, which describes the movement of water through the soil in steady infiltration as:

$$\frac{\partial}{\partial X}\left(K\frac{\partial \psi}{\partial X}\right)+\frac{\partial}{\partial z}\left(K\frac{\partial \psi}{\partial z}\right)+\frac{\partial K}{\partial Z}=S(X,Z,\psi) \tag{2}$$

where K= unsaturated hydraulic conductivity,ψ = suction potential, and S = root absorption function.

Richard's equation is a complex nonlinear equation involving the effects of pressure, soil porosity, and soils capacity to absorb water [8]. Studies about the equation have been done by numerous researchers. Haverkamp [9] using finite difference in order to solve transient unsaturated flow problems, Tian-Cheng [10] employing a multifield coupling discrete-element model. Clements [11] using Boundary Element Method (BEM) and Solekhudin [7] with Dual Reciprocity Boundary Element Method (DRBEM)

This study employs the DRBEM as used in [7]. DRBEM is an extension of the BEM. This method is an approach that involves discretizing the domain boundaries to evaluate integral equations [5]. DRBEM uses the concept of dual reciprocity to transform domain integral. This is achieved by approximating the domain terms using radial basis function or other interpolation function [13]. The advantage of DRBEM is considered capable of reducing computational burden by representing the solution only on the boundaries, simplifying the modeling process by directly modeling the boundary conditions, and being suitable for infiltration problems involving irregular boundaries [14].

Solekhudin [7] studied water infiltration from trapezoidal periodic channels with varying root absorption in homogeneous soil. The results showed suction potential values at each root ranging from -110 to -50 cm. The research was later developed by Solekhudin [8], changing the soil object to a three-layer heterogeneous type but without root absorption. The results showed suction potential values in the first soil layer diverging from -125 to -50 cm, the second soil layer more convergent to -125 cm, and the third soil layer converging to -200 cm. Solekhudin et al. Solekhudin [15] then studied infiltration with root absorption in a two-layer heterogeneous soil. The results showed suction potential values in the first layer diverging from -125 to -100 cm, and the second layer more convergent to -160 cm.

The research discussed in this study will develop these previous studies. The shape of the irrigation channel used in this study is rectangular, with both impermeable and non-impermeable conditions. Heterogeneous soil types are selected as four layers (Horizons O, A, B, and C) [16]. In addition to using DRBEM, this research also requires a predictor-corrector scheme, as used in [15] and [8]. The predictor-corrector scheme is an iterative method used to find numerical solutions for differential equations [17]. This study will then compare the water infiltration characteristics in the four-layer heterogeneous soils for rectangular types of furrow irrigation channels.

2. Basic Equation and Formulation

This research examines how water steadily seeps into a four-layer heterogeneous soil, Horizons O, A, B, and C, from rectangular channels under impermeable and non-impermeable conditions. Each channel has a specific width and depth. They are arranged in a repeating pattern.

The assumptions underlying this research are as follows:

1. The channels are always full of water, and infiltration only occurs at the surface of the irrigation channels.
2. Each irrigation channel is assumed to have a constant width and to be very long, with a uniform geometry along the Y-axis. Therefore, the length along the Y-axis can be neglected.
3. The irrigation channels are rectangular in shape, with a constant cross-sectional length of $2L$ for each channel.
4. Two adjacent channels, separated by a plant-covered surface, are $2(L+D)$ units apart from their respective center points.
5. A single row of plants is evenly spaced in the middle of the surface between two adjacent channels, with a root zone width of $2X_m$ and a root zone depth of Z_m.
6. The infiltration rate denoted as v_0 is constant at the surface of the irrigation channel.

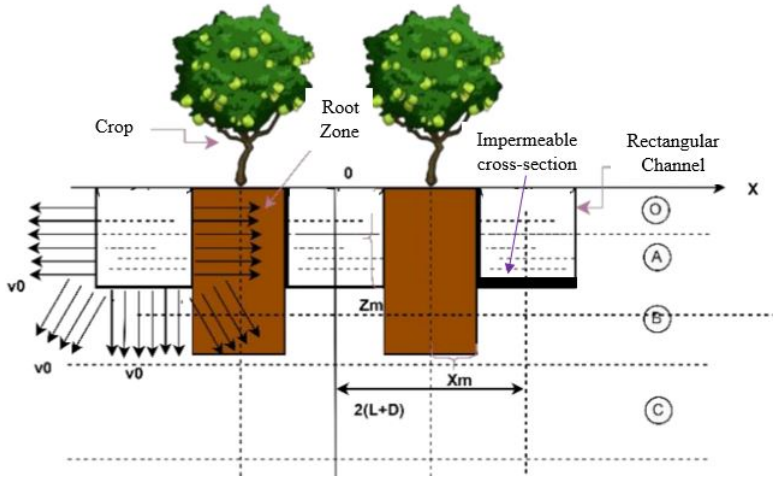

Figure 1. Geometry of Rectangular Channel at Furrow Irrigation Channels with Crops

Based on the assumptions, each irrigation channel exhibits symmetrical characteristics. The study area defined by $0 \leq X \leq L + D$ and $Z \geq 0$, is the focus of infiltration analysis. For this research, the length of $L = D$ is 50 cm. The infiltration flux at the channel surface is set at 0.75 times the value of saturated hydraulic conductivity.

2.1. Several Transformations

Implementation of DRBEM in Infiltration equation 2 can be solved by transforming the equation into a linear PDE form. Some transformations to simplify Richard's equation into a linear equation are as follows.

1. Kirchoff transformation
$$\Theta = \int_{-\infty}^{\psi} K(s)\, ds \tag{3}$$
Θ is the matric flux potential (MFP).
2. Exponential model of hydraulic conductivity
Given that α_1 is the soil parameter for horizon O, α_2 for horizon A, α_3 for horizon B, and α_4 for horizon C, then the average soil parameter value, denoted as α^*. Then, the exponential model of hydraulic conductivity is defined as
$$K = K_0^* e^{\alpha^* \psi}, \quad \alpha^* > 0 \quad (5) \tag{4}$$
and K_0^* is the average hydraulic conductivity of saturated heterogeneous soil.
3. Dimensionless Variables To eliminate the physical units from the equations, making them easier to analyze, the following is used:
$$x = \frac{\alpha^*}{2} X; \quad z = \frac{\alpha^*}{2} Z; \quad \Phi = \frac{\pi \Theta}{v_0 L}; \quad u = \frac{2\pi}{v_0 \alpha^* L} U; \quad v = \frac{2\pi}{v_0 \alpha^* L} V; \quad f = \frac{2\pi}{v_0 \alpha^* L} \tag{5}$$
v_0 is the initial flux. U and V are the fluxes in the horizontal and vertical directions, respectively.
4. Dimensionless Constants
The root water uptake utilized in equation 2 is based on the model presented in [41] and is defined as follows:
$$S(X, Z, h) = \gamma(h) \int_0^L \int_L^{L+D} \beta(X, Z) T_{pot}\, dX\, dZ \tag{6}$$

The function γ is the dimensionless response function for soil water stress, and it is defined as constant value follows [39]:

$$\gamma(h) = \begin{cases} -\frac{5}{8}h, & \text{for } -1.6 \leq h \leq 0 \\ 1, & \text{for } -4.7 < h < -1.6 \\ \frac{2}{7}h + \frac{82}{35}, & \text{for } -8.2 \leq h \leq -4.7 \end{cases}$$

L_t represents the width of the soil surface related to the transpiration rate, T_{pot} stands for the potential transpiration, and β is the modeled spatial distribution of root-water uptake, defined as:

$$\beta(X,Z) = \left(1 - \frac{Z}{Z_m}\right)\left(1 - \frac{L+D-X}{X_m}\right)e^{-K} \tag{7}$$

and

$$K = P_Z\,|Z^* - Z| + P_X\,|X^* - (L+D-X)|$$

Z_m, X_m, respectively indicate the depth and the half width of the root zone, the parameters P_Z, P_X, Z^*, and X^* are empirical in nature.
Equation 6 and 7 are transformed with dimensionless constant as below

$$\begin{aligned} lt = \ \frac{\alpha^*}{2}Lt; \quad x_m = \frac{\alpha^*}{2}X_m; \quad z_m = \frac{\alpha^*}{2}Z_m; \quad x^* = \frac{\alpha^*}{2}X^*; \\ z^* = \frac{\alpha^*}{2}Z^*; \quad a = \frac{\alpha^*}{2}L; \quad b = \frac{\alpha^*}{2}(L+D) \end{aligned} \tag{8}$$

5. Exponential Transformation

$$\Phi = \phi e^x \tag{9}$$

2.2. Modified Helmholtz Equation and Boundary Conditions

The final result of the transformation equation 2 using 6-9 is the modified helmholtz equation as follows:

$$\frac{\partial^2\phi}{\partial x^2} + \frac{\partial^2\phi}{\partial z^2} - \phi = \gamma^*(\phi)\, s_m^*(x,z)\, e^{-z} \tag{10}$$

where γ^* is the water stress response function and s_m^* is the sink term.

$$\gamma^*(\phi) = \gamma\left(\frac{1}{\alpha^*}\cdot\ln\left(\frac{\alpha^* v_0 L\phi e^z}{\pi K_0^*}\right)\right)$$

$$s_m^*(x,z) = \frac{2\pi}{v_0 L\alpha^*}\cdot\frac{l_t\tau^*(x,z)T_{pot}}{\int_0^{z_m}\int_{b-x_m}^{b}\tau^*(x,z)\,dx\,dz}$$

and the value:

$$\psi = \frac{1}{\alpha_n}\ln\left(\frac{v_0\alpha_n L\phi e^z}{\pi\sum_{i=1}^{n}(K_0^*)_i}\right)$$

$$\tau^*(x,z) = \left(1 - \frac{b-x}{x_m}\right)\left(1 - \frac{z}{z_m}\right)e^{-j}$$

For $b - x_m \leq x \leq b$, $0 \leq z \leq z_m$, where

$$j = 2\alpha^*\left(p_x x_m\,|x^* - (b-x)| + p_z z_m\,|z^* - z|\right)$$

with flux values:

$$f = un_1 + vn_2 = -e^z \frac{\partial \phi}{\partial x} n_1 + \left(2\phi e^z - e^z \left(\phi + \frac{\partial \phi}{\partial z} \right) \right) n_2$$

The normal derivative is obtained as follows:

$$\frac{\partial \phi}{\partial n} = \phi n_2 - e^{-z} f$$

The following are the boundary conditions for the non-impermeable irrigation channel derived based on the assumptions previously mentioned:

$$\begin{aligned}
\frac{\partial \phi}{\partial n} &= 2\pi \alpha L e^{-z} + \phi n_2, \text{ at the channel surface} \\
\frac{\partial \phi}{\partial n} &= -\phi, \text{ at the soil surface outside the channel} \\
\frac{\partial \phi}{\partial n} &= 0, \text{ for x} = 0 \text{ and z} \geq 0 \\
\frac{\partial \phi}{\partial n} &= 0, \text{ for x} = \text{b and z} \geq 0 \\
\frac{\partial \phi}{\partial n} &= -\phi, \text{ for } 0 \leq \text{x} \leq \text{b and z} = 4
\end{aligned} \tag{11}$$

Then, The difference for infiltration in an impermeable irrigation channel lies in the direction of water flow, which is only horizontal, with no downward flow. The boundary conditions for the impermeable irrigation channel are presented as below:

$$\begin{aligned}
\frac{\partial \phi}{\partial n} &= 2\pi \alpha L e^{-z} + \phi n_2, \text{ at the vertical channel surface} \\
\frac{\partial \phi}{\partial n} &= \phi n_2, \text{ at the horizontal channel surface} \\
\frac{\partial \phi}{\partial n} &= -\phi, \text{ at the soil surface outside the channel} \\
\frac{\partial \phi}{\partial n} &= 0, \text{ for x} = 0 \text{ and z} \geq 0 \\
\frac{\partial \phi}{\partial n} &= 0, \text{ forx} = \text{b and z} \geq 0 \\
\frac{\partial \phi}{\partial n} &= -\phi, \text{ for } 0 \leq \text{x} \leq \text{b and z} = 4
\end{aligned} \tag{12}$$

2.3. Implementation of DRBEM with predictor-corrector

The initial implementation of DRBEM was carried out without including the root absorption factor. A predictor-corrector scheme will be applied to the values of the water pressure response function (γ). As the name suggests, this scheme or method is divided into two phases: the predictor phase and the corrector phase. The predictor phase will provide an estimate of the initial value. The estimated value for the next step will use the value from the previous step. The next phase, the corrector, will refine the estimated value obtained from the predictor phase. Improving the accuracy of the estimated values requires additional information [21]. The four main steps of this scheme are Prediction-Evaluation-Correction-Evaluation [22]. This scheme will continue to iterate until the desired time interval is reached and specific convergence criteria are satisfied. Like other iterative methods, the error in the predictor-corrector scheme is obtained from the difference between the solution from the previous step and the current solution [23].

1. Implementation for infiltration problem in irrigation channels non-impermeable condition

The DRBEM can be used to numerically solve the two-dimensional boundary value problem 10 and 11 by reformulating them using the reciprocal relation as below.

$$\begin{aligned}\lambda(\xi,\eta)\phi(\xi,\eta) &= \int_{C_1}\left[\phi(x,z)\frac{\partial}{\partial n}\left(\Phi(x,z;\xi,\eta)\right)-\Phi(x,z;\xi,\eta)\left(2\pi\alpha L e^{-z}+\phi n_2\right)\right]ds(x,z)\\ &+\int_{C_2\cup C_5}\phi(x,z)\left[\frac{\partial}{\partial n}\left(\Phi(x,z;\xi,\eta)\right)+\Phi(x,z)\right]ds(x,z)\\ &+\int_{C_3\cup C_4}\phi(x,z)\frac{\partial}{\partial n}\left[\Phi(x,z;\xi,\eta)\right]ds(x,z)\\ &+\iint\Phi(x,z;\xi,\eta)\left[\phi(x,z)+\gamma^*(\phi)s_m^*(x,z)e^{-z}\right]dx\,dz\,R \end{aligned} \tag{13}$$

In this equation, $\Phi(x,z;\xi,\eta)$ is the fundamental solution to the two-dimensional Laplace equation. Equation 13 represents the integral solution to the infiltration equation, which is a modified Helmholtz equation $\phi(x,z)$ in R and

$$\lambda(\xi,\eta)=\begin{cases}1/2, & \text{for } (\xi,\eta) \text{ lies on the smooth part of the boundary}\\ 1, & \text{for } (\xi,\eta) \text{ belongs to the domain}\end{cases}$$

The primary step in implementing the DRBEM is constructing the linear equation system by taking collocation points on boundary N and interior domain$L$. These line segments are denoted as $C^{(1)}, C^{(2)}, \ldots, C^{(N)}$, with $(a^{(k)}, b^{(k)})$ representing the midpoint of each line segment for $k = 1, 2, \ldots, N$. The interior points are given by $(a^{(N+1)}, b^{(N+1)}), \ldots, (a^{(N+L)}, b^{(N+L)})$, and these are the collocation points used to numerically solve for ϕ in domain R and the closed curve C. The boundary integral equation 13 can be transformed into an algebraic equation system as follows:

$$\begin{aligned}\lambda(a^{(n)},b^{(n)})\phi^{(n)} &= \sum_{k=1}^{N}\phi^{(k)}\left[F_2^{(k)}(a^{(n)},b^{(n)})+\nu^{(k)}F_1^{(k)}(a^{(n)},b^{(n)})\right]\\ &-\sum_{k=1}^{N}f_l^{(k)}e^{-b^{(k)}}F_1^{(k)}(a^{(n)},b^{(n)})\\ &+\sum_{j=1}^{N+L}\mu(a^{(n)},b^{(n)};a^{(j)},b^{(j)})\left[\phi^{(j)}+\gamma^*(\phi)s_m^*(a^{(n)},b^{(n)})e^{-b^{(k)}}\right]\end{aligned} \tag{14}$$

for $n = 1, 2, \ldots, N + L$
Where:

$$\nu(k)=\begin{cases}0, & \text{if } C(k)\in C_3\cup C_4\\ 1, & \text{if } C(k)\in C_2\cup C_5\\ n_2, & \text{if } C(k)\in C_1\end{cases}$$

In this system: $\phi^{(n)}$ represents the value of ϕ evaluated at $a^{(n)}, b^{(n)}$,$f_l^{(k)}$ represents the flux at the collocation point $(a^{(k)}, b^{(k)})$, n_2 is the normal vector component on the Z-axis at the collocation point $(a^{(k)}, b^{(k)})$, which points outward from domain R.

$$
\begin{aligned}
F_1^{(k)}(a^{(n)},b^{(n)}) &= \frac{1}{4\pi}\int_{C^{(k)}} \ln\left((x-a^{(n)})^2+(z-b^{(n)})^2\right)\, ds(x,z)\\
F_2^{(k)}(a^{(n)},b^{(n)}) &= \frac{1}{4\pi}\int_{C^{(k)}} \frac{\partial \Phi}{\partial n}\left[\ln\left((x-a^{(n)})^2+(z-b^{(n)})^2\right)\right]\, ds(x,z)\\
\mu(a^{(n)},b^{(n)};a^{(j)},b^{(j)}) &= \sum_{m=1}^{N+L}\kappa(a^{(n)},b^{(n)};a^{(m)},b^{(m)})\cdot\omega(a^{(m)},b^{(m)};a^{(j)},b^{(j)})
\end{aligned}
$$

where:

$$
\begin{aligned}
\kappa(a^{(n)},b^{(n)};a^{(j)},b^{(j)}) &= \lambda(a^{(n)},b^{(n)})\cdot\chi(a^{(n)},b^{(n)};a^{(m)},b^{(m)})\\
&\quad+\sum_{k=1}^{N}\frac{\partial\chi(x,z;a^{(m)},b^{(m)})}{\partial n}\Big|_{(x,z)=(a^{(k)},b^{(k)})}F_1^{(k)}(a^{(n)},b^{(n)})\\
&\quad-\chi(a^{(k)},b^{(k)};a^{(m)},b^{(m)})F_2^{(k)}(a^{(n)},b^{(n)})\\
\omega(a^{(m)},b^{(m)};a^{(j)},b^{(j)}) &= \rho(a^{(j)},b^{(j)};a^{(m)},b^{(m)})^{-1}
\end{aligned}
$$

where:

$$
\chi(a^{(n)},b^{(n)};a^{(m)},b^{(m)}) = \frac{1}{4}r^2(a^{(n)},b^{(n)};a^{(m)},b^{(m)}) + \frac{1}{16}r^4(a^{(n)},b^{(n)};a^{(m)},b^{(m)}) + \frac{1}{25}r^5(a^{(n)},b^{(n)};a^{(m)},b^{(m)}),
$$

and:

$$
\rho(a^{(j)},b^{(j)};a^{(m)},b^{(m)}) = 1 + r^2(a^{(j)},b^{(j)};a^{(m)},b^{(m)}) + r^3(a^{(j)},b^{(j)};a^{(m)},b^{(m)}),
$$

where:

$$
r(a^{(j)},b^{(j)};a^{(m)},b^{(m)}) = \sqrt{(a^{(m)}-a^{(j)})^2+(b^{(m)}-b^{(j)})^2}.
$$

The function $\gamma^*(\varphi)$ can be determined using a predictor-corrector scheme, so it is assumed that $\gamma^*(\varphi)$ is constant. Thus, we obtain:

$$
\begin{aligned}
&\sum_{k=1}^{N}\left[(F_2^{(k)}(a^{(n)},b^{(n)})-\nu^{(k)}F_1^{(k)}(a^{(n)},b^{(n)}))\right]\varphi(k)+\sum_{j=1}^{N+L}\mu(a^{(n)},b^{(n)};a^{(j)},b^{(j)})\varphi(j)-\lambda(a^{(n)},b^{(n)})\varphi(n)\\
&=\sum_{k=1}^{N}f_l(k)e^{-b(k)}F_1^{(k)}(a^{(n)},b^{(n)})-\sum_{j=1}^{N+L}\mu(a^{(n)},b^{(n)};a^{(j)},b^{(j)})\left[\gamma^*(\varphi)sm^*(a^{(j)},b^{(j)})e^{-b(l)}\right]. \qquad (15)
\end{aligned}
$$

Equation 15 describes a system of linear equations (SPL) for the infiltration problem that incorporates root absorption. Due to its nonlinear nature, solving this system requires the use of a predictor-corrector method. This scheme is implemented to determine the value of $\gamma^*(\varphi)$, which simplifies equation (194) into a linear form. Consequently, solving for φ involves two primary steps. The first step entails solving SPL (194) without considering the sink term or root absorption to obtain an initial solution, φ_0. In the second step, SPL 15 is solved with the inclusion of the sink term or root absorption, where φ_0 serves as the predictor component and $\delta = \sum_{i=1}^{N+L}|\gamma_j^{*(i)} - \gamma_{j-1}^{*(i)}|$ functions as the corrector.

2. Implementation for infiltration problem in irrigation channels impermeable condition
The boundary conditions in Equations 12 are substituted into the Boundary Integral Equation resulting in:

$$\begin{aligned}\lambda(\xi,\eta)\varphi(\xi,\eta) &= \int_{C_1}\left[\varphi(x,z)\frac{\partial}{\partial n}\Phi(x,z;\xi,\eta)-\Phi(x,z;\xi,\eta)\left(2\pi\alpha Le^{-z}+\varphi_{n2}\right)\right]ds(x,z)\\ &+\int_{C_2}\left[\varphi(x,z)\frac{\partial}{\partial n}\Phi(x,z;\xi,\eta)-\Phi(x,z;\xi,\eta)\varphi_{n2}\right]ds(x,z)\\ &+\int_{C_3\cup C_6}\varphi(x,z)\left[\frac{\partial}{\partial n}\Phi(x,z;\xi,\eta)+\Phi(x,z;\xi,\eta)\right]ds(x,z)\\ &+\int_{C_4\cup C_5}\varphi(x,z)\frac{\partial}{\partial n}\left[\Phi(x,z;\xi,\eta)\right]ds(x,z)\\ &+\iint_R\Phi(x,z;\xi,\eta)\left[\varphi(x,z)+\gamma^*(\varphi)\,s_m^*(x,z)e^{-z}\right]dx\,dz. \end{aligned}\tag{16}$$

where $\Phi(x,z;\xi,\eta)$ is the fundamental solution to the two-dimensional Laplace equation. Analogous to the impermeable channel, the algebraic equation system based on equation 16 is obtained as follows:

$$\begin{aligned}\lambda(a^{(n)},b^{(n)})\varphi^{(n)} &= \sum_{k=1}^{N}\left[F_2^{(k)}(a^{(n)},b^{(n)})+\nu^{(k)}F_1^{(k)}(a^{(n)},b^{(n)})\right]\\ &-\sum_{k=1}^{N}f_l^{(k)}e^{-b^{(k)}}F_1^{(k)}(a^{(n)},b^{(n)})+\sum_{j=1}^{N+L}\mu(a^{(n)},b^{(n)};a^{(j)},b^{(j)})\\ &\left[\varphi^{(j)}+\gamma^*(\varphi)s_m^*(a^{(n)},b^{(n)})e^{-b^{(k)}}\right]\end{aligned}\tag{17}$$

for $n=1,2,\ldots,N+L$
where:

$$\nu(k)=\begin{cases}0, & C(k)\in C_4\cup C_5\\ 1, & C(k)\in C_3\cup C_6\\ n_2, & C(k)\in C_1 \text{ or } C_2\end{cases}$$

Then $F_1^{(k)}(a^{(n)},b^{(n)})$ and $F_2^{(k)}(a^{(n)},b^{(n)})$ are as previously defined. Since the same form of algebraic equation system is obtained, the solution process remains identical to that for the channel without impermeability.

The numerical solution of the Helmholtz Equation using DRBEM combined with the predictor-corrector scheme will be aided by MATLAB programming language. Some required input variables for running the program include the endpoints of line segments, flux on the line segments, boundary condition types, and interior collocation points. Meanwhile, the output variables consist of numerical solutions at the required points along with their graphical representations. The numerical solution obtained from the MATLAB program represents the suction potential (ψ). Subsequently, the obtained ψ values need to be validated by comparison with previous research findings. The final step of the research involves analyzing the results based on the validated MATLAB program output. Based on the analysis conducted, conclusions are obtained.

3. Experimental results

The approach described in the previous section is used to solve steady infiltration problems from periodic rectangular channels into heterogeneous soils consisting of four different layers with root-water uptake processes under non-impermeable and impermeable conditions. We justify the adopted parameter set $\mathbf{p}_{\text{base}}$ as follows:

1. **Physical plausibility.** All ψ values remain negative (unsaturated suction), and $\theta_r < \theta_s$ with porosity bounds respected; resulting $K(\psi)$ is monotone and within the reported soil-type ranges.
2. **Consistency with literature/site data.** Baseline $\{K_0^{(\ell)}, \alpha^{(\ell)}, n^{(\ell)}\}$ fall within reported intervals for the corresponding soil textures assigned to layers $\ell = 1, \ldots, 4$.
3. **Sensitivity-informed parsimony.** Parameters with low S_i^{T} are fixed at baseline values to reduce identifiability issues; high-influence parameters are prioritized for calibration.
4. **Predictive robustness.** Small perturbations (5–10%) in high-ranked parameters yield bounded changes in Q; the final calibrated set lies in regions where S_i^{T} is moderate, enhancing robustness to uncertainty.

The channel's cross-sectional length and the bed's cross-section are 1 meter. Assumed that the fluxes across the channel surfaces are constant, represented by v_0. The four-layered heterogeneous soils are YLC-CC-YFSL-GL. The upper two layers YLC-CC have a depth of 1/2 meter in each, and the lower two layers YFSL-GL have a depth of 1 meter in each soil structure. This research data is divided into two parts, one related to soil and the other to roots.

Table 1. Research Data Related to Soil

Horizon	Depth (cm)	Soil Texture	α (cm^{-1})	K_0 (cm/day)
O	$0-50$	Yolo Light Clay (YLC)	1.9×10^{-2}	1.063
A	$51-100$	Chino Clay (CC)	2.05×10^{-2}	1.98
B	$101-200$	Yolo Fine Sandy Loam (YFSL)	2.5×10^{-2}	3.52
C	$201-300$	Guelph Loam (GL)	3.4×10^{-2}	31.7088

The depth of each horizon is based on the literature [18]. The soil parameters (α) and hydraulic conductivity (K_0) for Chino Clay are from the literature [19]. Yolo Light Clay, Yolo Fine Sandy Loam, and Guelph Loam are from the literature [20]. Other assumptions related to the roots, such as parameters and coordinate values, are adapted from reference [7]. Based on the values in Table 1, the values of α^* = $2.4625 \times 10^{-2}\, cm^{-1}$ and K_0^* = $9.5679\, cm/day$ were obtained. This study also includes root water uptake, where the volume of water absorbed by the roots is utilized as a sink term represented by a factor for the water holding capacity that moves through the soil. Research data relating to the root zone are $X_m = 50\, cm$, $Z_m = 100\, cm$, $L_t = 50\, cm$, $X^* = 20\, cm$, $Z^* = 25\, cm$, $p_Z = 5.0$, $p_X = 2.0$

The numerical solution obtained from the MATLAB program is in the form of suction potential (ψ). Subsequently, the obtained values of ψ need to be validated to confirm the accuracy of the results. The validation is carried out by comparing them with previous studies, as in Solekhudin (2018), The suction potential values for infiltration without root absorption in soil layer 1 diverge from -125 to -50 cm, soil layer 2 converge more towards -125 cm, and soil layer 3 converge towards -200 cm. In addition, based on the existing theory, suction potential, which represents the matric suction of unsaturated soil, always has a negative value [2].

To obtain the numerical results, the discretization process used $N = 261$ boundary points and $M = 609$ interior points. With the specified parameters, elements, and interior points, the DRBEM with a predictor-corrector scheme, as outlined in the previous section, was employed to compute the numerical solutions. The solution process of the model uses a predictor-corrector scheme to estimate the value of γ, resulting in an error of 0.000098 for the non-impermeable channel and 0.000021 for the impermeable channel. The final numerical results are the suction potential values. Here are the results of suction potential values at several points of the non-impermeable irrigation channel

Figure 2 shows the graph of suction potential at several X points along the Z axis under non-impermeable conditions. In Horizon O, the suction potential at X=10 cm, specifically at the channel surface, is the highest

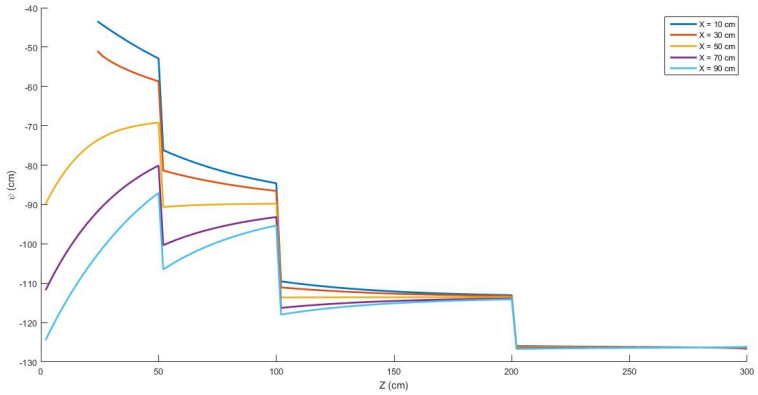

Figure 2. Graphs of ψ at selected values of X along Z-axis under non-impermeabel condition

compared to the other points. Conversely, at X=90 cm, particularly at the channel surface, it is the lowest. This indicates that the highest suction potential is found closest to the channel center, while the lowest occurs at the farthest point from the channel on the soil surface. Additionally, it can be observed that the suction potential values at each point are still widely spread. Horizons A and B also show the highest suction potential at X=10 cm and the lowest at X=90 cm. Based on the graph, the suction potential in Horizon A is still divergent but more concentrated than in Horizon O. In Horizon B, the values begin to converge. The suction potential in Horizon C has already reached convergence at a specific value. Upon closer inspection of the graph, each horizon displays jumps in suction potential values. Horizon O has the highest suction potential, followed by Horizon A, Horizon B, and the lowest in Horizon C. These results are influenced by variations in soil texture. Coarser soils, as indicated by higher soil parameters and greater saturated hydraulic conductivity values, tend to have lower suction potential values.

Table 2. Suction Potential Values at Several Points of the Non-Impermeable Irrigation Channel

Layer	X (cm)	Z (cm)	Soil Texture	Suction Potential (cm)
Horizon O	10	30	YLC	-45.90847532
	10	40	YLC	-49.65698602
Horizon A	10	60	CC	-78.17211851
	10	80	CC	-82.00000851
Horizon B	10	130	YFSL	-111.32015488
	10	140	YFSL	-111.74650334
Horizon C	10	260	GL	-126.23179080
	10	280	GL	-126.33834650
Horizon O	90	30	YLC	-98.35049456
	90	40	YLC	-92.05709290
Horizon A	90	60	CC	-103.66808004
	90	80	CC	-98.53547364
Horizon B	90	130	YFSL	-115.94626634
	90	140	YFSL	-115.48091744
Horizon C	90	260	GL	-126.41699190
	90	280	GL	-126.33789555

Table 2 presents the suction potential values at X = 10, directly beneath the channel, and at X = 90, farther from the channel, for various soil horizons. The initial analysis is for $X = 10$. In Horizon O, with Yolo Light Clay (YLC) from $Z = 30$ to $Z = 40$, the suction potential decreases by approximately 8.16%. Horizon A, with

Chino Clay (CC) from $Z = 60$ to $Z = 80$, shows a reduction of about 4.90%. Horizon B, with Yolo Fine Sandy Loam (YFSL) from $Z = 130$ to $Z = 140$, experiences a decrease of about 0.38%, with the difference becoming smaller. Horizon C, with Guelph Loam (GL) from $Z = 260$ to $Z = 280$, shows a decrease of about 0.08%, with the difference becoming negligible and the values tending to equalize.

The following analysis is for $X = 90$. In Horizon O, with Yolo Light Clay (YLC) from $Z = 30$ to $Z = 40$, the suction potential increases by about 6.40%. Horizon A, with Chino Clay (CC) from $Z = 60$ to $Z = 80$, shows an increase of approximately 4.95%. Horizon B, with Yolo Fine Sandy Loam (YFSL) from $Z = 130$ to $Z = 140$, exhibits a 0.40% increase, with the difference becoming smaller. Horizon C, with Guelph Loam (GL) from $Z = 260$ to $Z = 280$, displays a decrease of about 0.06%, with the difference being small and the values tending to stabilize.

The analysis suggests that in Horizons O and A, the suction potential decreases with increasing depth, and the rate of decrease becomes smaller as Z increases. In Horizons B and C, the suction potential values tend to stabilize, converging towards a specific value. Conversely, at points farther from the channel, the suction potential increases with depth, but the increase diminishes as Z rises, and the values stabilize in Horizons B and C.

Figure 3 displays suction potential and root-water uptake function at several X points along the Z axis under impermeable conditions. Horizon O exhibits the highest suction potential at X = 50 cm in comparison to the other points. In contrast, at X = 90 cm, particularly at the channel surface, the value is the lowest. This finding suggests that the greatest suction potential occurs between the channel and the surface, while the lowest suction potential is found at the point farthest from the channel on the soil surface. This differs from the previous scenario due to the presence of an impermeable layer at the channel's base, which leads to more water accumulating above the channel.

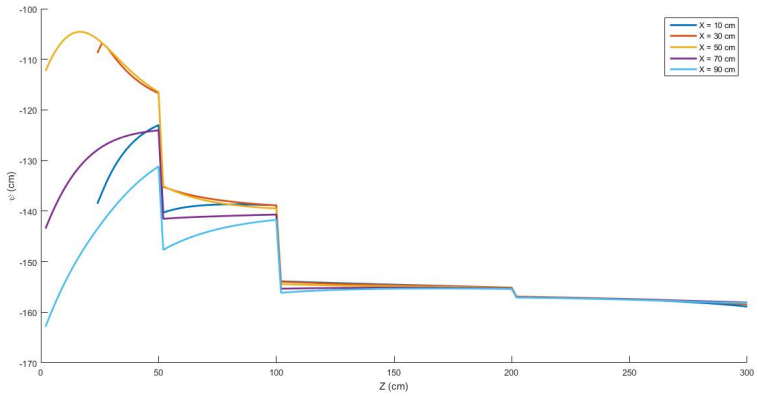

Figure 3. Graphs of ψ and S at selected values of X along Z-axis under impermeabel condition

Moreover, it is evident that the suction potential values at each point remain quite dispersed. Horizon A also shows the highest suction potential at X = 50 cm and the lowest at X = 90 cm. As shown in the graph, the suction potential at Horizon A remains divergent but is somewhat more concentrated than Horizon O. In contrast, at Horizon B, the values are beginning to converge. Finally, the suction potential values at Horizon C have fully converged to a specific value. The graph reveals that each Horizon shows a significant change in suction potential values. Horizon O has the highest suction potential, while Horizon C has the lowest. This variation is influenced by soil texture differences. The coarser the soil, as reflected in soil parameters and higher saturated hydraulic conductivity, the lower the suction potential value.

Table 3 presents the suction potential values at two distinct points along the Z-axis: X = 10 (directly beneath the channel) and X = 90 (far from the channel), across different soil horizons. The first analysis focuses on X = 10. At this point, Horizon O, composed of Yolo Light Clay (YLC) from Z = 30 to Z = 40, exhibits an increase in suction potential by approximately 4.74%. In contrast, Horizon A, which consists of Chino Clay (CC) from Z = 60 to Z = 80, shows a decrease in suction potential of around 0.48%. Horizon B made up of Yolo Fine Sandy Loam (YFSL) from Z = 130 to Z = 140, experiences a slight increase of 0.09%, with the difference becoming less pronounced.

Table 3. Suction Potential Values at Several Points of the Impermeable Irrigation Channel

Layer	X (cm)	Z (cm)	Soil Texture	Suction Potential (cm)
Horizon O	10	30	YLC	-132,27432984
	10	40	YLC	-126,00989546
Horizon A	10	60	CC	-139,34240503
	10	80	CC	-138,67659859
Horizon B	10	130	YFSL	-154,27736575
	10	140	YFSL	-154,41077875
Horizon C	10	260	GL	-157,64530984
	10	280	GL	-158,11777428
Horizon O	90	30	YLC	-139,85816268
	90	40	YLC	-134,81406635
Horizon A	90	60	CC	-145,84571834
	90	80	CC	-143,06975116
Horizon B	90	130	YFSL	-155,51469030
	90	140	YFSL	-155,40950601
Horizon C	90	260	GL	-157,65537600
	90	280	GL	-157,95131827

Horizon C, containing Guelph Loam (GL) from Z = 260 to Z = 280, shows a decrease of about 0.30%, with the differences becoming negligible and values tending to stabilize.

The second analysis examines X = 90. For this point, Horizon O with Yolo Light Clay (YLC) from Z = 30 to Z = 40 shows a 3.60% increase in suction potential. Horizon A, consisting of Chino Clay (CC) from Z = 60 to Z = 80, demonstrates a 1.90% increase. Horizon B with Yolo Fine Sandy Loam (YFSL) from Z = 130 to Z = 140 shows a very small increase of 0.07%, with the difference becoming smaller. Finally, Horizon C, which contains Guelph Loam (GL) from Z = 260 to Z = 280, experiences a small decrease of 0.18%, with the difference being minor and values stabilizing. This analysis indicates that the suction potential tends to vary in both magnitude and direction across different soil horizons, depending on the distance from the channel and the soil's characteristics.

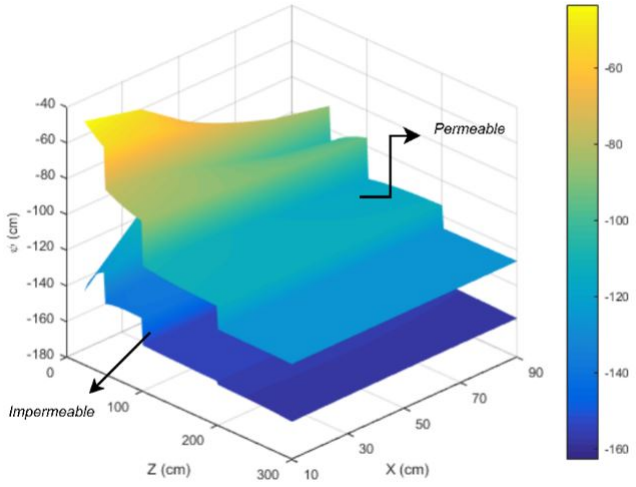

Figure 4. Graphs of ψ and S at selected values of X along Z-axis under impermeabel condition

Next is the analysis comparing the suction potential values at impermeable and non-impermeable irrigation channels. According to Table 5, the suction potential range for the permeable irrigation channel is broader, with a minimum of -126.70 cm and a maximum of -43.42 cm. In contrast, the impermeable channel has a narrower range,

with a minimum of -162.85 cm and a maximum of -104.56 cm. This difference is due to the design of permeable channels, which facilitate larger-scale infiltration. Higher suction potential values correspond to a greater amount of water being absorbed, resulting in increased water content in the soil.

Table 4. Comparison of Suction Potential Values for Each Horizon in Permeable and Impermeable Irrigation Channels

Channel Condition	**Horizon**	**Soil Texture**	ψ **(cm) Minimum**	ψ **(cm) Maximum**
Non-impermeable	O	YLC	-87.05	-43.42
	A	CC	-106.52	-76.19
	B	YFSL	-117.97	-109.54
	C	GL	-126.70	-125.96
Impermeable	O	YLC	-162.85	-104.56
	A	CC	-147.66	-135.06
	B	YFSL	-156.15	-153.88
	C	GL	-158.87	-156.89

Figures 5a and 5b respectively show root water uptake in non-impermeable and impermeable soils for $0 \leq Z \leq 100$ and $X = 55, 65, 75, 85, 95\, cm$. In this case, based on the Zm parameter, the maximum rooting zone is known to be 100 cm deep, so the analysis is carried out on the soil layers of horizon O to A. The maximum value of S was observed at $X = 75$ cm, particularly at (75 cm, 20 cm). Values of S decreased slightly at $X = 85$ cm and $X = 95$ cm compared to the peak at $X = 75$ cm. Conversely, S values at $X = 55$ cm and $X = 65$ cm, equidistant from $X = 75$ cm, were significantly lower. This suggests that water absorption by roots is higher closer to the plant at a depth of $Z = 20$ cm. For YLC-CC at a depth of 50 cm, there were significant increases in S at certain X values, particularly at 75 cm, 85 cm, and 95 cm. These increases in S correspond to heterogeneous soil in the values of 50 cm.

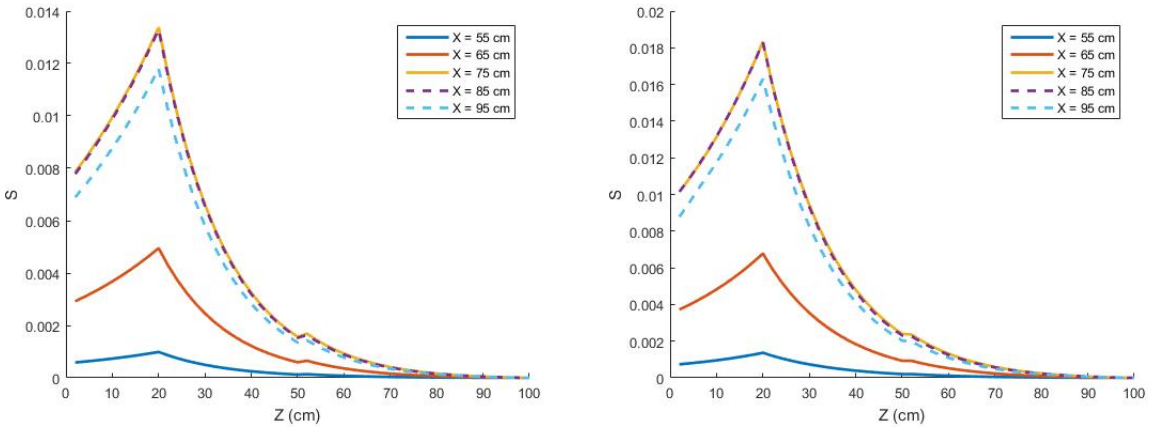

Figure 5. a. b. Graphs of S at selected values of X along Z-axis under non-impermeabel and impermeabel condition

The strong influence of $K_0^{(1)}$ and $\alpha^{(1)}$ in the uppermost soil layer suggests that channel bed permeability critically governs early infiltration. In the Indonesian context, where irrigation is often carried out through unlined earthen channels, this finding translates into: channel lining or partial compaction to reduce excessive seepage in highly permeable soils, controlled infiltration zones, where increased permeability is deliberately maintained to recharge local groundwater aquifers in regions facing water scarcity. Thus, DRBEM outputs provide a scientific basis for determining where to line channels and where to preserve natural infiltration.

Parameters $\alpha^{(*)}$ reflecting the importance of root-zone hydrodynamics. This can be translated into practical strategies such crop selection based on rooting depth, shallow-rooted crops (e.g., paddy) depend heavily on

optimized surface layers, while deep-rooted crops (e.g., sugarcane, maize) benefit from stable water storage in deeper layers.

4. Conclusion

The mathematical model of the infiltration problem in this study has been solved using the implementation of DRBEM with a combination of predictor-corrector schemes. The obtained numerical solution represents the suction potential values. The characteristics of water infiltration in the four soil layers or horizons, influenced by varying root absorption, show different behaviors. Based on the obtained numerical solution, the movement of water from the upper layer diverges until it converges in the bottom layer. This indicates that the suction potential from the upper layer initially moves from varying values until it eventually approaches or converges to a single value. The jumps in suction potential values for each horizon are caused by differences in soil texture. The coarser the soil texture, the smaller the suction potential value. Meanwhile, the numerical solution for non-impermeable channels tends to be higher compared to impermeable ones. This is because non-impermeable channels are designed for larger-scale infiltration. Higher suction potential values indicate greater water absorption, which in turn leads to an increase in soil water content.

The results can be observed through graphs of suction potential values. The suction potential at Horizon O (YLC) is highly divergent, whereas Horizon A (CC) shows divergence, but it becomes more convergent. Horizon B (YFSL) is approaching convergence, and Horizon C (GL) is fully convergent. Initially, the suction potential values from the topsoil layer vary, but they eventually converge towards a single value. These variations and jumps in suction potential for each horizon are due to differences in soil texture. Specifically, coarser soils tend to have smaller suction potential values.

Furthermore, the comparison between impermeable and permeable irrigation channels reveals that the suction potential is generally higher in permeable channels. Higher suction potential values indicate increased water absorption and a higher water content in the soil. This observation suggests that permeable channels facilitate greater infiltration than impermeable ones.

Acknowledgements

This activity was carried out with the support of the Institute of Research and Community Service of the University of Jember (LP2M UNEJ) through the Internal Grant for the Beginner Research Program, based on the Dean's Decree of the University of Jember Number: 6274/UN25/KP/2025 dated March 17, 2025, and the Assignment Agreement Number: 2770/UN25.3.1/LT/2025 dated March 17, 2025.

REFERENCES

1. B.C. Chun, K. Hong, S. Sohn, and H. Hwnag, *El Nino southern oscillation affects on influenza peak activity seasons: comparison of the effects between Korea and the USA with surveillance data from 2005 to 2018*, International Journal of Infectious Diseases, vol. 79, 2019.
2. Chen, X. W., Wong, J. T. F., Wang, J. J., Ng, C. W. W., & Wong, M. H, *Effects of mycorrhizal Bermuda grass on low-range soil matric suction*, *Journal of Soils and Sediments*, 21(2), 2021.
3. C. Li, Y. Feng, T. Sun, and X. Zhang, *Long Term Indian Ocean Dipole (IOD) Index Prediction Used Deep Learning by convLSTM*. Remote Sens (Basel), vol. 14, no. 3, 2022.
4. M. Ehteram et al., *Performance improvement for infiltration rate prediction using hybridized Adaptive Neuro-Fuzzy Inferences System (ANFIS) with optimization algorithms*, Ain Shams Engineering Journal, vol. 12, no. 2, 2021.
5. J. T. Katsikadelis, The Boundary Element Method for Engineers and Scientists, 2nd, Amsterdam: Elsevier, 2016.
6. M. Manaqib, *Pemodelan Matematika Infiltrasi Air pada Saluran Irigasi Alur*, Jurnal Matematika "MANTIK," vol. 3, no. 1, 2017.
7. I. Solekhudin, *Water infiltration from periodic trapezoidal channels with different types of root-water uptake*, Far East Journal of Mathematical Sciences, vol. 100, no. 12, pp. 2029–2040, Dec. 2016.
8. I. Solekhudin, N. H. Malysa, Sumardi, and A. Zulijanto, *A Numerical Study of Steady Water Absorption by Plant Roots in Heterogeneous Soils* , International Journal of Mathematical and Computational Methods, vol. 4, 2019.

9. Haverkamp, R., Vauclin, M., Touma, J., Wierenga, P. J. *A comparison of numerical simulation models for one-dimensional infiltration*, Soil Science Society of America Journal, 41(2),1 285-294, 1977.
10. Tian, C., Cheng, Y., Li, H. *Numerical simulation of soil-water-air interaction in unsaturated soils using a coupled discrete element method,* Computers and Geotechnics, 122, 2020.
11. D. L. Clements, M. Lobo, and N. Widana, *A hypersingular boundary integral equation for a class of problems concerning infiltration from periodic channels,* Electronic Journal of Boundary Elements, vol. 5, pp. 1–16, 2007.
12. M. Zahroh, *Penentuan Jenis Fungsi Basis Radial dalam Dual Reciprocity Boundary Element Method,* Majalah Ilmiah Matematika dan Statistika, vol. 21, no. 1, p. 53, Mar. 2021
13. P. W. Partridge, C. A. Brebbia, and L. C. Wrobel, *The Dual Reciprocity Boundary Element Method*, Computational Mechanics Publications, 1992.
14. J. H. Cushman and D. M. Tartakovsky, The handbook of groundwater engineering: Third edition. 2016.
15. I. Solekhudin, *Steady Infiltration in Heterogeneous Soil,* in Journal of Physics: Conference Series, 2018.
16. X. Ji, E. Abakumov, V. Tomashunas, V. Polyakov, and S. Kouzov *Geochemical pollution of trace metals in permafrost-affected soil in the Russian Arctic marginal environment,* Environ Geochem Health, vol. 42, no. 12, 2020
17. Z. Odibat and N. Shawagfeh, *An optimized linearization-based predictor-corrector algorithm for the numerical simulation of nonlinear FDEs,* Phys Scr, vol. 95, no. 6, 2020,
18. D. S. Subardja, S. Ritung, M. Anda, E. Suryani, and R. E. Subandiono *Petunjuk Teknis Klasifikasi Tanah Nasional*. 2014.
19. H. Zhan *Advances in Groundwater Flow and Solute Transport*, Pushing the Hidden Boundary, Mdpi AG, 2019.
20. J. E. Ayars, D. Zaccaria, and K. M. Bali *Microirrigation for Crop Production: Design, Operation, and Management*, Elsevier Science, 2023.
21. D. Gruyter Numerical Methods, De Gruyter, 2019.
22. S. J. Fletcher, *Semi-lagrangian advection methods and their applications in geoscience,* 2019.
23. W. Liu and W. Guo, *A novel predictor–corrector explicit integration scheme for structural dynamics,* Structures, vol. 34, 2021
24. M. U. Gul, A. Paul, S. Manimurugan, and A. Chehri, *Hydrotropism: Understanding the Impact of Water on Plant Movement and Adaptation,* Water (Switzerland), vol. 15, no. 3. 2023.